www.rericjournal.ait.ac.th

Sensitivity Analysis of Electrochemical Model Parameters for Lead-acid Batteries

Haizhou Ren[*], Kailang Dong[+1], Jiasen Li[+], Lei Chen[*], Hongfei Zhao[#], and Zhiyan Zhang[^]

ARTICLE INFO

Article history:
Received 28 September 2025
Received in revised form
09 March 2026
Accepted 17 April 2026

Keywords:
Battery management
Electrochemical model
Lead acid batteries
Parameter sensitivity analysis
Parameter benchmark

ABSTRACT

A high-precision electrochemical model of lead-acid batteries is the core foundation for enhancing the safety of battery management systems. However, the numerous parameters and strong coupling characteristics of the model make identification difficult. In order to explore the design basis for an efficient and accurate parameter identification framework, this paper conducted a parameter sensitivity analysis. The parameter value ranges for 23 variables were determined based on established lead-acid battery literature. The sensitivity analyses were then performed across different C-rates and depth of discharge regions, primarily evaluating parameter identifiability. Additionally, the impact of parameter uncertainty on critical model outputs, specifically electrolyte concentration and side reaction overpotential, was quantified under constant-current charging conditions. The results indicate that capacity and electrochemically relevant parameters with high sensitivity significantly influence the terminal voltage. Accordingly, this paper proposes a stepwise identification strategy and clarifies the optimal identification conditions for different parameters: capacity-related parameters are suitable for low-current conditions, while electrochemical parameters require identification under high-rate currents.

1. INTRODUCTION

Lead-acid batteries have been identified as a mature, cost-effective electrochemical energy storage technology with a well-established recycling system. This has led to the conclusion that they play a crucial role in ensuring the safe and stable operation of power systems [1]. In the context of hydropower plants, these systems function as backup power sources. They facilitate the initiation of black start operations by providing initial energy and ensure the continuity of power supply to control and protection systems during primary power outages. The reliability and lifespan of these components have a direct impact on the operational safety of hydropower units and even regional power grids [2], [3]. However, actual battery operation involves factors like continuous charge-discharge cycles, different C-rates, and long-term float charging. These can cause capacity degradation and increased internal resistance. Ultimately, they may result in a reduced lifespan and even thermal runaway risks. It is imperative to meticulously monitor the battery states, encompassing state of charge (SOC) [4], state of health (SOH) [5], [6], and state of power (SOP) [7]. The accuracy of estimating and predicting these states depends on the utilization of a high-performance battery management system.

At present, the core algorithms in battery management systems are predominantly based on equivalent circuit models. Equivalent circuit models are well-suited to real-time monitoring, due to their simple structure, high computational efficiency, and ease of online parameter identification. However, equivalent circuit models do not adequately address the mechanisms of nonlinear electrochemical processes within batteries, resulting in suboptimal accuracy in long-term degradation behavior, responses under extreme conditions, and side reactions such as gas evolution. This complicates the fulfilment of battery safety management requirements throughout the entire lifecycle. In order to surmount this limitation, there is an urgent necessity to develop battery management systems based on electrochemical models. Electrochemical models offer high precision and can provide insights into internal physical processes, thus constituting the foundation for next-generation battery management system (BMS) [8]. However, the high precision of electrochemical models depends on the accuracy of the parameters employed. Electrochemical models are characterized by a high number of parameters, and experimental identification is a time-consuming and

DOI: https://doi.org/10.64289/iej.26.0206.4128296

[*] Xiaolangdi Multipurpose Dam Project Management Center, MWR, Zhengzhou 450004, China

[+] State Grid Henan Extra High Voltage Company, Zhengzhou, 450000, China

[#] State Grid Jiangsu Electric Power Co., Ltd. Ultra High Voltage Branch, Nanjing 211102, China

[^] School of Electrical and Information Engineering, Zhengzhou University of Light Industry, Zhengzhou, 450002, China

[1]Corresponding author
E-mail: 1738645688@qq.com

labor-intensive process. This is further complicated by the fact that some parameters exhibit time-varying characteristics. Consequently, the identification of parameters through the utilization of artificial intelligence algorithms has garnered considerable attention. Nevertheless, this data-driven parameter identification is confronted with some challenges, including the curse of dimensionality and the risk of overfitting [9], [10]. Parameter sensitivity analysis is a process that can be utilized to identify critical sensitive parameters and guide the design of identification conditions, so this analysis is considered a necessary prerequisite [11]. Parameter sensitivity analysis has been widely applied to various battery models [11–14].

In their seminal study, Hojat et al.[12] proposed a probabilistic model, grounded in the sparse Jacobi polynomial chaos expansion to quantify the uncertainty of lead-acid batteries. Then they proceeded to perform a global sensitivity ranking of 19 parameters using the Sobol index. Nevertheless, the parameter ranges under consideration lack sufficient supporting literature and have been conservatively set. Li et al. [11] determined the boundary ranges of the 26 parameters in their model based on literature on ternary lithium batteries and conducted parameter sensitivity analysis under dynamic operating conditions, finding that capacity-related parameters had a more significant impact than the other parameters. Chen [13] proposed a distinguishability analysis framework to study the effects that model parameters have on voltage and temperature outputs. Furthermore, the framework was designed to examine the effects of critical operating conditions on model parameters. It is important to acknowledge that the aforementioned studies have all concentrated on lithium-ion battery systems. Igor et al. [14] developed a straightforward and universally applicable solid-state battery model, and they conducted a comprehensive analysis of its parameters. Their findings revealed that the electrolyte diffusion coefficient exerts a substantial influence on the efficiency of the battery. Nevertheless, the present study is chiefly concerned with the design and optimization of battery materials.

In order to address the aforementioned research gap, this paper conducted a sensitivity study on the electrochemical model parameters of lead-acid batteries for battery management systems. A total of 23 parameters were determined based on publicly available lead-acid battery parameters as typical values. In the course of constant-current charge-discharge experimentation, encompassing various C-rates and depth of discharge (DOD) regions, the sensitivity effects of parameters on four safety-critical states were quantitatively assessed including terminal voltage, electrolyte concentration, oxygen evolution overpotential at the positive electrode, and hydrogen evolution overpotential at the negative electrode. This work provides a foundation for experimental design and identification strategies for battery model parameter identification.

The following sections are contained within this paper, in addition to the introduction: the second section of this study introduces the electrochemical model of lead-acid batteries. The third section describes the calibration of model parameters for lead-acid batteries. The fourth section outlines the objectives and methodology of parameter sensitivity analysis. The fifth section presents the results of parameter sensitivity analysis and discusses implications for parameter identification. Finally, the sixth section concludes the paper.

2. LEAD-ACID BATTERIES ELECTROCHEMI - CAL MODEL

As shown in Figure 1, a lead-acid battery consists of five components: positive electrode, acid storage compartment, separator, negative electrode and current collector. During charging and discharging, chemical reactions occur at the positive and negative electrodes (see Equations 1 and 2). During discharge, PbO_2 at the positive electrode and Pb at the negative electrode react electrochemically to form $PbSO_4$. Upon charging, the $PbSO_4$ reverts to PbO_2 and Pb through the reverse reaction. Since the reaction involves solid-phase transformation, the active surface area of the electrode's changes during charge and discharge, as shown in Equation (3).

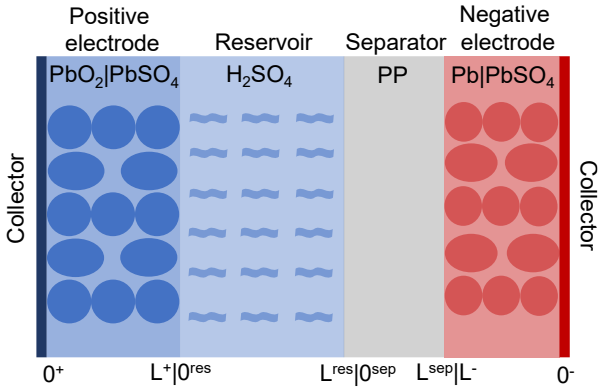

Fig. 1. Schematic of the electrochemical model for Lead-acid batteries.

$$PbO_2 + HSO_4^- + 3H^+ + 2e^- \underset{\text{charge}}{\overset{\text{discharge}}{\rightleftharpoons}} PbSO_4 + 2H_2O \quad (1)$$

$$Pb + HSO_4^- \underset{\text{charge}}{\overset{\text{discharge}}{\rightleftharpoons}} PbSO_4 + H^+ + 2e^- \quad (2)$$

$$\begin{cases} A = A_{max}\left(\dfrac{\varepsilon-\varepsilon_0}{\varepsilon_{\max}-\varepsilon_0}\right)^{\xi} & \text{(Discharge)} \\ A = A_{max}\left(\dfrac{\varepsilon-\varepsilon_0}{\varepsilon_{\max}-\varepsilon_0}\right)^{\xi}\left(\dfrac{\varepsilon_{\max}-\varepsilon}{\varepsilon_{\max}-\varepsilon_0}\right) & \text{(Charge)} \end{cases} \quad (3)$$

Where A_{max} is maximum electroactive area, A is electroactive area, ε is porosity, ε_0 is zero charge porosity, ε_{max} is fully charged porosity, ζ is morphology parameter on kinetics, with a value of 2.

During charge and discharge, the phase transformation among PbO_2, Pb, and $PbSO_4$, which is driven by differences in their molar volumes, leads to changes in the porous structure of the electrodes. This,

in turn, affects the solid-phase conductivity, liquid-phase conductivity, and the rate of mass diffusion in the electrolyte, with the specific relationships given in Equation (4).

$$\sigma^{\text{eff}}=\sigma(1-\varepsilon)^{\tau_s},k^{\text{eff}}=k\varepsilon^{r_l},k_D^{\text{eff}}=k_D\varepsilon^{r_l},D^{\text{eff}}=D\varepsilon^{\tau_l} \quad (4)$$

where ε is porosity, τ_s=0.5, $r_l=\tau_l$=1.5.

During operation, lead-acid batteries undergo changes in the porosity of the active material, and in the solid-phase electronic conductivity, liquid-phase ionic conductivity and electrolyte diffusion. Due to their large aspect ratio, these phenomena can be described using partial differential equations in a one-dimensional model. The specific derivation of these equations can be found in [15], and the formulas are summarized in Table 1. The parameters in the formulas are detailed in Tables 2 and 3.

Table 1. Summary of control equations for electrochemical models of lead-acid batteries.

Physics variables	Governing equations
Porosity	$\frac{\partial\varepsilon}{\partial t}=a_1\frac{Aj}{2F}$, $a_1^+=\left(\frac{M_{\text{PbSO}_4}}{\rho_{\text{PbSO}_4}}-\frac{M_{\text{PbO}_2}}{\rho_{\text{PbO}_2}}\right)$, $a_1^-=\left(\frac{M_{\text{Pb}}}{\rho_{\text{Pb}}}-\frac{M_{\text{PbSO}_4}}{\rho_{\text{PbSO}_4}}\right)$
Solids potential	$\nabla\cdot\left(\sigma^{\text{eff}}\nabla\phi_s\right)=Aj$
Liquid potential	$\nabla\cdot\left(\kappa^{\text{eff}}\nabla\phi_e\right)+\nabla\cdot\left(\kappa_D^{\text{eff}}\nabla\ln c\right)=-Aj$, $K_D=\frac{RT\kappa}{F}\left(2t_+^0-1\right)$
Electrolyte concentration	$\frac{\partial(\varepsilon c)}{\partial t}=\nabla\cdot\left(D^{\text{eff}}\nabla c\right)+a_2\frac{Aj}{2F}$, $a_2^+=\left(3-2t_+^0\right)$, $a_2^-=\left(1-2t_+^0\right)$
Exchange current density	$j=i_0\left(\frac{c}{c_{ref}}\right)^{\gamma}\left[\exp\left(\frac{\alpha_a F\eta}{RT}\right)-\exp\left(-\frac{\alpha_c F\eta}{RT}\right)\right]$, $\eta=\phi_s-\phi_e-\Delta U$

3. PARAMETER BENCHMARKING FOR LEAD-ACID BATTERIES

Electrochemical models involve numerous parameters and any change to which can affect the model's output. For the results of parameter sensitivity analysis to be reliable, a reasonable parameter range is required. Therefore, this section identifies typical values for 23 key parameters. These values are based on the literature in lead-acid battery electrochemical modelling with defined ranges for different parameters. The table shows the ranges of the 23 electrochemical parameters determined in this study and their sources. To facilitate subsequent analysis and discussion of the results, these parameters have been categorized into four groups based on their physical meaning and how they function within the model.

(1) Geometric parameters

The model uses 9 parameters to characterize the geometric features of the battery. These include the width of the electrode and the acid storage chamber, as well as the porosity of the electrode and separator. These parameters directly determine the volume of active material in the electrode, thereby affecting the battery's theoretical capacity.

(2) Transport parameters

This paper conducts a sensitivity analysis of 3 transport parameters, including positive and negative electrode electronic conductivity and ion mobility. These parameters influence the ohmic and concentration polarization of the battery.

(3) Kinetic parameters

The model's Kinetic parameters are primarily derived from the Butler-Volmer (B-V) equation, comprising a total of 10 parameters. These parameters can be divided into 4 categories, including exchange current density, maximum active area, charge transfer coefficient and charge transfer reaction concentration index. These parameters characterize the electrochemical reactions that occur during charging and discharging of the battery and influence its electrochemical polarization.

(4) Concentration parameters

In this paper, the electrochemical model uses the initial electrolyte concentration as the concentration parameter. Similar to the geometric parameters, these parameters are related to the battery capacity; however, it primarily affects the battery's actual usable capacity.

In addition to the 23 aforementioned parameters, the model incorporates two further categories of parameters. The first category consists of physical constants with universally accepted standard values, such as the density of lead and lead dioxide, for which the variation ranges do not require determination. The second category comprises polynomial functions associated with electrolyte concentration, including the electrolyte diffusion coefficient and electrolyte conductivity. These parameters are typically obtained through experimental fitting, and the analysis of such parameters falls outside the scope of this study. The two categories of parameters utilized in this model are outlined in Table 3.

Table 2. List of electrochemical model parameter value ranges for the sensitivity analysis.

Category	Symbol	Unit	Description	Benchmarking	Boundaries
Geometric parameters	L^+	cm	Positive electrode thickness	0.0865[16], 0.16685[17], 0.06[18,19] , 0.09[20]	0.06-0.16685
	L^{res}	cm	Reservoir thickness	0.16[16,18], 0.055[16,18,19], 0.13[17]	0.055-0.16
	L^{sep}	cm	Separator thickness	0.056[16], 0.2[16], 0.014[16,18,19], 0.07[17]	0.014-0.07
	L^-	cm	Negative electrode thickness	0.0815[16,18,19], 0.075[16], 0.06[16,18,19] 0.138[17], 0.125[20]	0.06-0.125
	ε^+_{max}	-	Positive electrode fully charged porosity	0.55[16,18], 0.565[16], 0.53[16,18,19], 0.57[20]	0.53-0.57
	ε^+_0	-	Positive electrode zero charged porosity	0.28[17], 0.27[17], 0.34[21]	0.28-0.34
	ε^{sep}	-	Separator porosity	0.6[16,18], 0.73[16,18,19], 0.58[17], 0.92[20]	0.58-0.92
	ε^-_{max}	-	Negative electrode fully charged porosity	0.61[16,18], 0.63[16], 0.53[16],[18–20]	0.53-063
	ε^-_0	-	Negative electrode zero charged porosity	0.31[17], 0.3[21]	0.3-0.31
Transport parameters	σ^+	S cm^{-1}	Positive electrode conductivity	80[16–20], 500[16]	80-500
	σ^-	S cm^{-1}	Negative electrode conductivity	48000 [16],[18–20], 47000[17]	47000-48000
	t^+_0	-	Transfer number of H^+	0.9[16,18], 0.72[16–21]	0.72-0.9
Kinetic parameters	i^+_o	A cm^{-2}	Positive electrode exchange current density	6×10^{-7} [16,18,20], 6.66×10^{-7} [16], 1.5×10^{-7} [17]	1.5×10^{-7}- 6.66×10^{-7}
	i^-_o	A cm^{-2}	Negative electrode exchange current density	8×10^{-6} [16,18,20], 2.5×10^{-6} [17]	2.5×10^{-6}- 8×10^{-6}
	A^+_{max}	cm^2 cm^{-3}	Positive electrode maximum electroactive area	2.05×10^5 [16,18], 2.3×10^5 [16,17], 2×10^5[17]	2×10^5-2.3×10^5
	A^-_{max}	cm^2 cm^{-3}	Negative electrode maximum electroactive area	2.5×10^4[16,18], 2.3×10^4[16,17], 2×10^4[17]	2×10^4-2.5×10^4
	α^+_a	-	Anodic charge transfer coefficient, positive electrode	0.7[16] , 0.5[16] , 1.15[18]	0.5-1.15
	α^+_c	-	Cathodic charge transfer coefficient, positive electrode	1.3[16], 0.85[18], 0.5[16]	0.5-1.3
	α^-_a	-	Anodic charge transfer coefficient, negative electrode	1[16], 1.55[18], 0.5[16]	0.5-1.55
	α^-_c	-	Cathodic charge transfer coefficient, negative electrode	1[16], 0.45[18], 0.5[16]	0.5-1
	γ^+	-	Charge transfer reaction concentration exponent, positive electrode	0.5[16], 0.3[18], 1.5[16]	0.3-1.5
	γ^-	-	Charge transfer reaction concentration exponent, negative electrode	0.5[16], 1.0[18], 1.5[16]	0.5-1.5
Concentration parameters	c_0	mol m^{-3}	Initial electrolyte concentration	4.8×10^{-3} [18], 4.1×10^{-3} [16], 4.9×10^{-3} [16]	4.1×10^3- 4.9×10^3

Table 3. Physical constants and other parameters.

Symbol	Unit	Description	Value
ρ_{Pb}	g cm^{-3}	Density of Pb	11.34
ρ_{PbO2}	g cm^{-3}	Density of PbO_2	9.7
ρ_{PbSO4}	g cm^{-3}	Density of $PbSO_4$	6.3
M_{Pb}	g mol^{-1}	Relative molecular mass of Pb	207.2
M_{PbO2}	g mol^{-1}	Relative molecular mass of PbO_2	239.2
M_{PbSO4}	g mol^{-1}	Relative molecular mass of $PbSO_4$	303.26
	κ,s cm^{-1}	Electrolyte conductivity [20]	$c\exp(6.23-134c-16100c^2)$
	D ,cm s^{-1}	Electrolyte diffusion coefficient [20]	$(175+260.0c)\times10^{-9}$

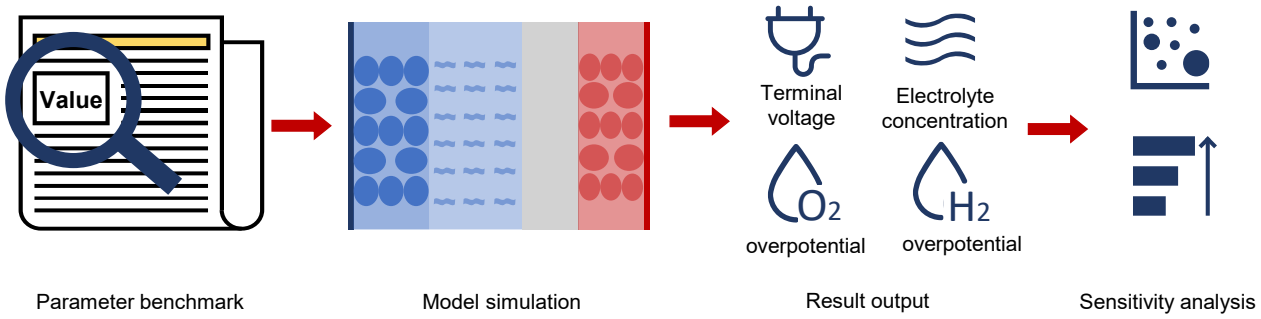

Fig. 2. Framework of parameter sensitivity analysis.

4. PARAMETER SENSITIVITY ANALYSIS

The parameter sensitivity analysis process is illustrated in Figure 2. The parameters vary within the ranges determined in Section 3, and the electrochemical model outputs various results under different operating conditions. The final step in the process is the calculation of the parameter sensitivity index. This section is principally concerned with the introduction of the target state of parameter sensitivity analysis, the parameter value strategy, and the sensitivity calculation index.

4.1 Target State of Parameter Sensitivity Analysis

The parameter sensitivity analysis provides a foundation for a parameter identification framework, which aims to ensure the predictive accuracy of electrochemical models in battery management systems. The most frequently employed external signal in BMS is voltage; consequently, analyzing the impact of parameter changes on terminal voltage is of the utmost importance. The model employed in this study is an electrochemical model, which confers the key advantage of providing insight into the internal state of the battery. Consequently, it is imperative to direct attention towards internal states, including electrolyte concentration, oxygen evolution overpotential, and hydrogen evolution overpotential.

4.1.1 Terminal voltage

The terminal voltage is the most direct signal utilized by BMS for state estimation and power regulation control. The low-cost measurability of battery terminal voltage makes it a common data source for parameter identification. The sensitivity of parameters to terminal voltage is also considered to be a measure of their identifiability. The terminal voltage simulated by the lead-acid electrochemical model is shown in Equation (5).

$$V(t)=\phi_s\left(0^+,t\right)-\phi_s\left(0^-,t\right) \tag{5}$$

Where V(t) is the battery terminal voltage, which is obtained by subtracting the solid-state potentials ϕ_s at the 0^+ and 0^- positions shown in Figure 1.

4.1.2 Electrolyte concentration

In the electrochemical model of lead-acid batteries, the electrolyte is understood to primarily refer to the concentration of hydrogen ions or sulfate ions. In circumstances where the electrolyte concentration in the acid storage compartment is high, the battery's effective usable capacity is constrained. The electrolyte concentration under consideration in this paper is the average concentration in the acid storage compartment, calculated as shown in Equation (6).

$$c_1(t)=\frac{1}{N_x^{res}}\sum_{i=1}^{N_x^{res}}c_i^{res}(t) \tag{6}$$

Where N_x^{res} is the number of grids in the acid storage chamber calculation area, i.e., the 0^{res}~L^{res} region in Figure 1, and c_i^{res} is the electrolyte concentration value at the i-th grid point.

4.1.3 Side reaction overpotential

The overpotentials examined in this paper primarily encompass oxygen evolution overpotential and hydrogen evolution overpotential. Oxygen evolution and hydrogen evolution are defined as side reactions that occur during the charging and discharging process of

lead-acid batteries. It is evident that these reactions have a significant impact on two key aspects of the battery: charging efficiency and remaining life. Furthermore, a close relationship between these reactions and battery safety has been established. The calculation methods for these two potentials in the electrochemical model are shown in Equations (7) and (8).

$$\eta_{o_2}(x,t) = \phi_s(x,t) - \phi_e(x,t) - \Delta U_{o_2} \quad (7)$$

$$\eta_{H_2}(x,t) = \phi_s(x,t) - \phi_e(x,t) - \Delta U_{H_2} \quad (8)$$

Where η_{o_2} and η_{H_2} are the overpotentials for oxygen evolution and hydrogen evolution, respectively, which are related to the rates of their side reactions. ϕ_e is the liquid phase potential. ΔU_{o_2} = 1.23 V, and ΔU_{H_2} = 0 V. The oxygen evolution and hydrogen evolution reactions primarily occur at the anode and cathode, respectively, due to the differences in electrode working potentials. Therefore, this paper analyzes the sensitivity of $\eta_{o_2}(L^+,t)$ and $\eta_{H_2}(L^-,t)$.

4.2 Methodology for Parameter Sensitivity Analysis

Parameter sensitivity analysis quantifies the impact of parameter uncertainty on model outputs, through the definition of a parameter sampling strategy and the calculation of sensitivity indices. In this study, the parameter sensitivity analysis employs a one-at-a-time method, meaning that only one parameter is varied at a time. It is important to note that each parameter varies within the range determined in Section 3 for the electrochemical model parameters of lead-acid batteries. The values of the parameters follow a uniform distribution, as demonstrated in the following equation. During this parameter variation process, the remaining parameters are set to their median values, as demonstrated in Equations (9) and (10).

$$p_i = p_l + (i-1)\frac{p_u - p_l}{N_s} \quad (9)$$

$$\bar{p} = \frac{p_l + p_u}{2} \quad (10)$$

Where p_i is the i-th value of the parameter, p_l is the minimum value of the parameter, p_u is the maximum value of the parameter, N_s is set to 10 in this paper, meaning that the parameter changes ten times in total, and $\bar{p}$ is the reference value.

Lead-acid batteries used in hydropower stations typically operate in either constant current discharge or float charge modes.Therefore, the present study conducts a parameter sensitivity analysis under constant current charge-discharge conditions. In circumstances involving constant current discharge conditions, the primary function of lead-acid batteries is to supply power for lighting and control systems. The following discharge C-rates are considered, including 0.5C (114.64 A/m²), 1C (229.28 A/m²), and 2C (458.56 A/m²). However, under constant current discharge conditions, the lead-acid battery is predominantly in a float charge state, and thus a charging current density of 13.49 A/m² is considered. In order to calculate the parameter sensitivity under different conditions, the voltage curve output by the model when all parameters are set as reference values is used as a baseline. The root mean square (RMS) of the voltage after parameter changes relative to the baseline is calculated, as demonstrated in Equation (11).

$$\mathrm{SI} = \sqrt{\frac{1}{N_s}\sum_{i=1}^{N_s}\left(x_i - x_{ref}\right)^2} \quad (11)$$

Where SI is the sensitivity index, i is the i-th parameter value, x_i is the target state output by the model simulation, and x_{ref} is the model output when all the parameters are set to their reference values.

It is evident that varying charge and discharge C-rates exert an influence on the internal state of the battery. Furthermore, it has been demonstrated that differing SOC regions also affect the internal state of the battery. From the perspective of parameter identification, the use of a reduced number of voltage segments has been shown to enhance the efficiency of the process and to prevent overfitting. Consequently, this study also calculates the parameter sensitivity of different SOC regions. The considered SOC regions range from 0 to 1, with each region being 0.2, thus resulting in a total of five regions, as illustrated in Equation (12).

$$\mathrm{ASI}(\mathrm{ASOC}) = \sqrt{\frac{1}{N_s}\sum_{i=1}^{N_s}\left(x_i(\mathrm{ASOC}) - x_{ref}(\mathrm{ASOC})\right)^2} \quad (12)$$

Where ASOC is 0~0.2, 0.2~0.4, 0.4~0.6, 0.6~0.8, and 0.8~1.

5. RESULTS AND DISCUSSION

The subject of this study is lead-acid batteries utilized in hydroelectric power plants. These batteries do not directly interact with the power grid and are typically used for fixed loads such as lighting and control systems. Consequently, the parameter sensitivity analysis is chiefly concerned with constant current conditions. The analysis employs the electrochemical model outlined in Section 2, utilizing a total of 920 model runs to execute the parameter sensitivity analysis.

5.1 Parameter Sensitivity Analysis under Constant Current Discharge Conditions

In order to analyze parameter sensitivity under constant current discharge conditions, different parameter values and discharge C-rates were set using MATLAB 2023a, and the simulation model was run 690 times in COMSOL 6.3. All the simulations were conducted until the battery terminal voltage reached the preset discharge cutoff voltage of 1.8V. The present analysis primarily explored the impact of varying discharge C-rates and DOD regions on parameter sensitivity.

In order to analyze the impact of differing model parameters on the output voltage of the model, Figure 3 presents the results of the sensitivity analysis for 16 parameters e.g., L^+, L^{res}, L^{sep}, ε^+_{max}, ε^+_0, ε^{sep}, σ^+, t^+_0, i^+_o, A^+_{max}, α^+_a, α^+_c, α^-_a, α^-_c, γ^+, and c_0, under the 1C

constant current discharge condition. The 16 parameters encompass all physical regions and parameter categories of the model. The results of the sensitivity analysis for each parameter are presented in separate subplots, with each subplot containing 11 voltage-time curves. The orange curve signifies the reference voltage value, with the remaining ten curves depicting the results for the corresponding parameter at ten distinct values. The parameter values are varied from the minimum value (corresponding to the blue curve) to the maximum value (corresponding to the red curve), as indicated by the arrows and color gradients in the subplots.

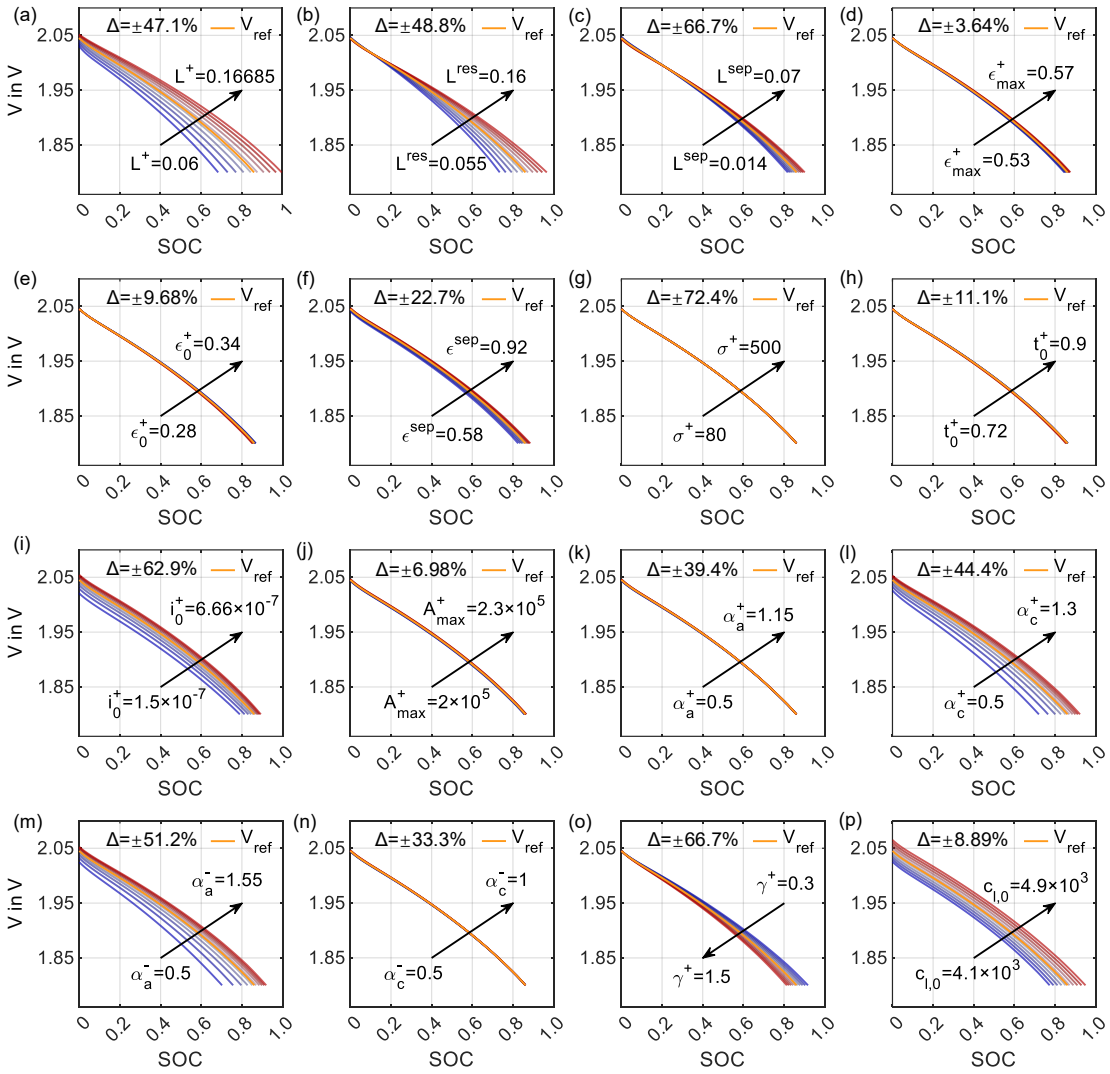

Fig. 3. Sensitivity analysis of 16 parameters under 1C constant current discharge conditions. (a) Results of L^+, (b) Results of L^{res}, (c) Results of L^{sep}, (d) Results of ε^+_{max}, (e) Results of ε^+_0, (f) Results of ε^{sep}, (g) Results of σ^+, (h) Results of t^+_0, (i) Results of i^+_o, (j) Results of A^+_{max}, (k) Results of α^+_a, (l) Results of α^+_c, (m) Results of α^-_a, (n) Results of α^-_c, (o) Results of γ^+, (p) Results of c_0.

As illustrated in Figure 3, among the 16 parameters under consideration, the voltage curve shifts significantly relative to the reference curve when these nine parameters e.g., L^+, L^{res}, L^{sep}, ε^{sep}, i^+_o, α^+_c, α^-_a, γ^+, and c_0 take different values. It is widely acknowledged within the scientific community that parameters which exhibit a substantial impact on the discharge voltage are to be regarded as highly sensitive parameters [11], [13]. Based on the offset characteristics, these nine parameters can be categorized into two distinct groups.

The first category comprises five parameters e.g., L^+, i^+_o, α^+_c, α^-_a, and c_0, exert a substantial influence on the initial end voltage value and discharge termination time of the discharge process. The discharge curve tends to deviate toward the arrow direction when the parameter values are modified.Among the five parameters under consideration, three of them e.g., i^+_o, α^+_a, and α^+_c, are electrochemical parameters. Notably, one of the two remaining parameters, e.g., c_0, originates from concentration parametersbut appears in the Butler-Volmer equation, indicating its relevance to electrochemical reactions. Although L^+ from geometric parameters, it influences exchange current density distribution and similarly relates to electrochemical reactions.

The second category comprises four parameters e.g., L^{res}, L^{sep}, ε^{sep}, and γ^+, which primarily affect voltage by altering the discharge termination time. L^{res} is a capacity-related parameter, as its value increases, the discharge termination time is delayed. However, it has been demonstrated that both L^{sep} and ε^{sep} exert an

indirect influence on the available capacity of the battery, accomplished through the modification of the battery's internal resistance, consequently affecting the discharge termination time. Despite the fact that γ^+ is an electrochemical parameter, its contribution weight in the B-V equation is relatively low. Consequently, it only affects the discharge termination time.

The preceding analysis demonstrates that all nine highly sensitive parameters are classified as either electrochemical or geometric parameters. Among the seven remaining low-sensitivity parameters, α_a^+, α_c^-, and A_{max}^+ are electrochemical in nature.However, these parameters exhibit a significantly lower influence on discharge voltage than would be predicted. It is evident that α_a^+ and α_c^- correspond to the oxidation reaction at the cathode and the reduction reaction at the anode, respectively. However, during discharge, the cathode undergoes a reduction reaction, and the anode undergoes an oxidation reaction. A_{max}^+ demonstrates low sensitivity owing to its restricted range of variation, with a change amplitude of ±6.98% relative to its median value. In contrast, i_0^+, which is also an electrochemical parameter, has a change amplitude of ±62.9%. Geometric parameters ε_{max}^+ and ε_0^+ demonstrate low sensitivity for the same reason as A_{max}^+. Electrochemical model parameters demonstrate high sensitivity in two distinct conditions. Firstly, the parameter displays a considerable range of values; secondly, the parameter is associated with the dominant electrochemical reaction under operating conditions or capacity-related parameters. In the process of parameter identification, the parameters that meet both of these conditions should be prioritized.

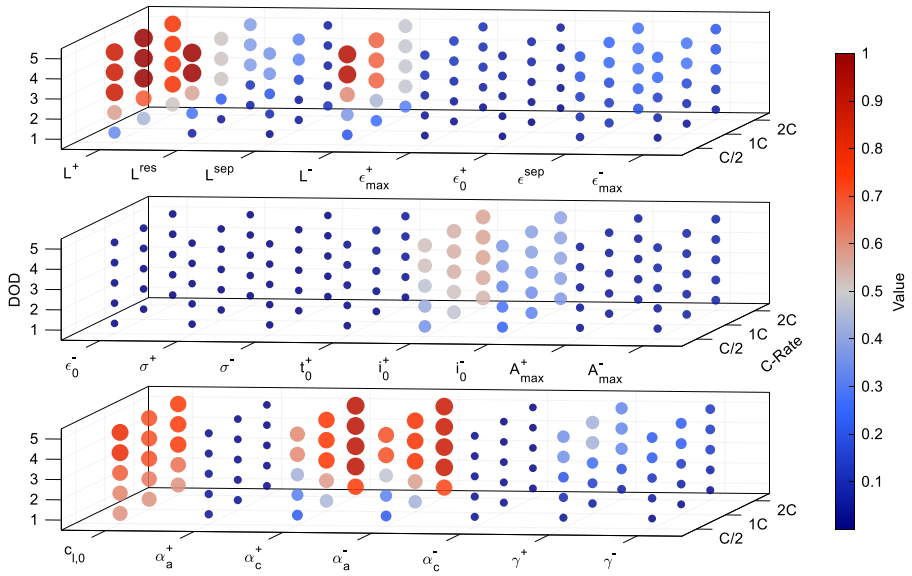

Fig. 4. Parameter sensitivity analysis of different discharge C-rates and discharge region depth.

The results of the parameter sensitivity analysis for different discharge C-rates and depth of discharge regions are shown in Figure 4. The figure is composed of three sub-figures, with the x-axis representing parameter identifiers, the y-axis representing discharge current rates, and the z-axis representing corresponding DOD regions, e.g., "1" corresponds to the initial discharge stage where SOC ranges from 1 to 0.8. The normalized sensitivity index is represented by the color and size of the bubbles. From a parameter perspective, the two high-sensitivity parameter conditions summarized above remain applicable under different discharge C-rates. It has been demonstrated that the parameters which fail to meet these conditions consistently exhibit low sensitivity.

From the perspective of discharge C-rate, the sensitivity index of electrochemical parameters increases significantly with increasing C-rate. This phenomenon can be attributed to the observation that, under high C-rate discharge conditions, there is an increase in the current density. In turn, this results in a significant enhancement of electrochemical polarization, which is associated with interfacial reactions. According to the B-V equation, even minor alterations in parameters can induce substantial overpotential changes under conditions of strong polarization, resulting in more pronounced terminal voltage shifts. However, it has been demonstrated that the sensitivity index of capacity-related parameters decreases with increasing C-rate[22]. In conditions of low current, this phenomenon occurs because the battery terminal voltage is predominantly influenced by the open-circuit voltage. The shape of the latter is associated with the parameters that are related to capacity. However, as the C-rate increases, the contribution of electrochemical polarization to the terminal voltage increases and becomes the dominant factor, resulting in a corresponding decrease in the sensitivity index of the terminal voltage to capacity-related parameters. From the perspective of the DOD, at the stage near the end of discharge (DOD=5), the sensitivity index of the high-sensitivity parameters further significantly increases to its maximum. The low-sensitivity parameters have not exhibited any discernible alterations.

In general, electrochemical parameters exhibit higher sensitivity indices under high C-rate conditions, thereby offering superior identifiability under such conditions. However, capacity-related parameters

demonstrate enhanced identifiability under low C-rate conditions, attributable to their substantial influence on open-circuit voltage. It has been demonstrated that, for both high-sensitivity electrochemical and capacity parameters, the utilization of voltage curve segments at the termination of the discharge process for identification analysis is a more efficient approach. Furthermore, the analysis results demonstrate that low-sensitivity parameters show low sensitivity across a range of C-rates and DOD regions, indicating poor identifiability. The subsequent section (Section 5.2) will provide a detailed discussion of the impact of such parameters' uncertainty on the accuracy of model output predictions.

5.2 Parameter Sensitivity Analysis Under Constant Current Charging Conditions

The present section is concerned with the analysis of the impact on parameter uncertainty under charging conditions. The charging cutoff time is set to 270 seconds. As demonstrated in Figure 5, the sensitivity of the four parameters, e.g., L^-, σ^-, i_o^+, and c_0, is depicted. The figure illustrates how different values of these parameters affect the four target states , e.g., $\smile$, c_l, η_{O_2}, and η_{H_2}. Increasing L^- results in a shift of the terminal voltage curve downward to the right, while the negative electrode hydrogen evolution overpotential curve shifts upward to the left. The effect of L^- on electrolyte concentration is negligible. The parameter under consideration has been found to exert negligible influence on the oxygen evolution overpotential. This is consistent with the mechanism underpinning the oxygen evolution reaction, which has been established to occur primarily at the positive electrode [23]. Furthermore, σ^- has been determined to have a negligible effect on all four output states. This is a typical low-sensitivity parameter. Terminal voltage and oxygen evolution overpotential are substantially affected by an increase in i_o^+. Both the curves exhibit right-shift characteristics accompanied by voltage depression.The effect of i_o^+ on electrolyte concentration and hydrogen evolution overpotential is relatively insignificant. c_0, as an initial condition, has an observable effect on all four output states.

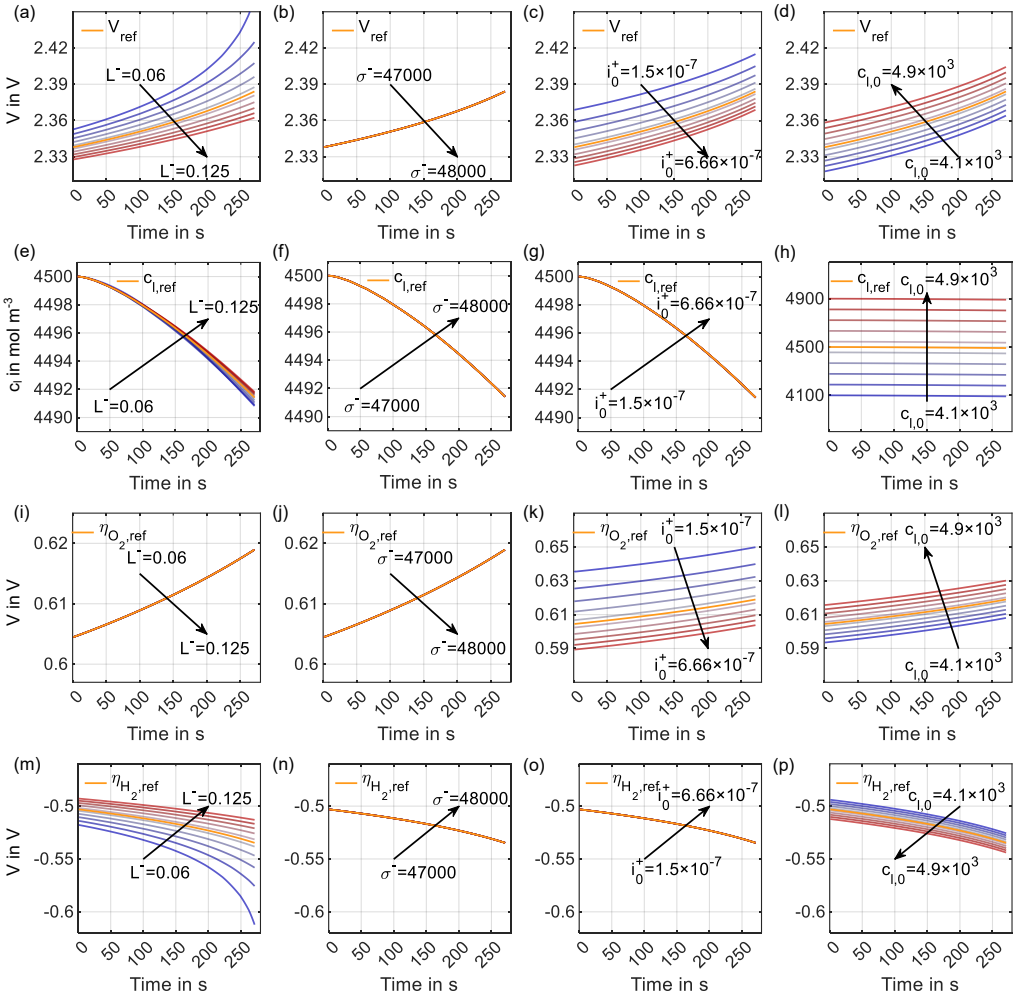

Fig. 5. Sensitivity analysis of four parameters under constant-current charging conditions. (a) Results of L^- for terminal voltage. (b) Results of σ^- for terminal voltage. (c) Results of i_o^+ for terminal voltage. (d) Results of c_0 for terminal voltage. (e) Results of L^- for electrolyte concentration. (f) Results of σ^- for electrolyte concentration. (g) Results of i_o^+ for electrolyte concentration. (h) Results of c_0 for electrolyte concentration. (i) Results of L^- for oxygen evolution overpotential. (j) Results of σ^- for oxygen evolution overpotential. (k) Results of i_o^+ for oxygen evolution overpotential. (l) Results of c_0 for oxygen evolution overpotential. (m) Results of L^- for hydrogen evolution overpotential. (n) Results of σ^- for hydrogen evolution overpotential. (o) Results of i_o^+ for hydrogen evolution overpotential. (p) Results of c_0 for hydrogen evolution overpotential.

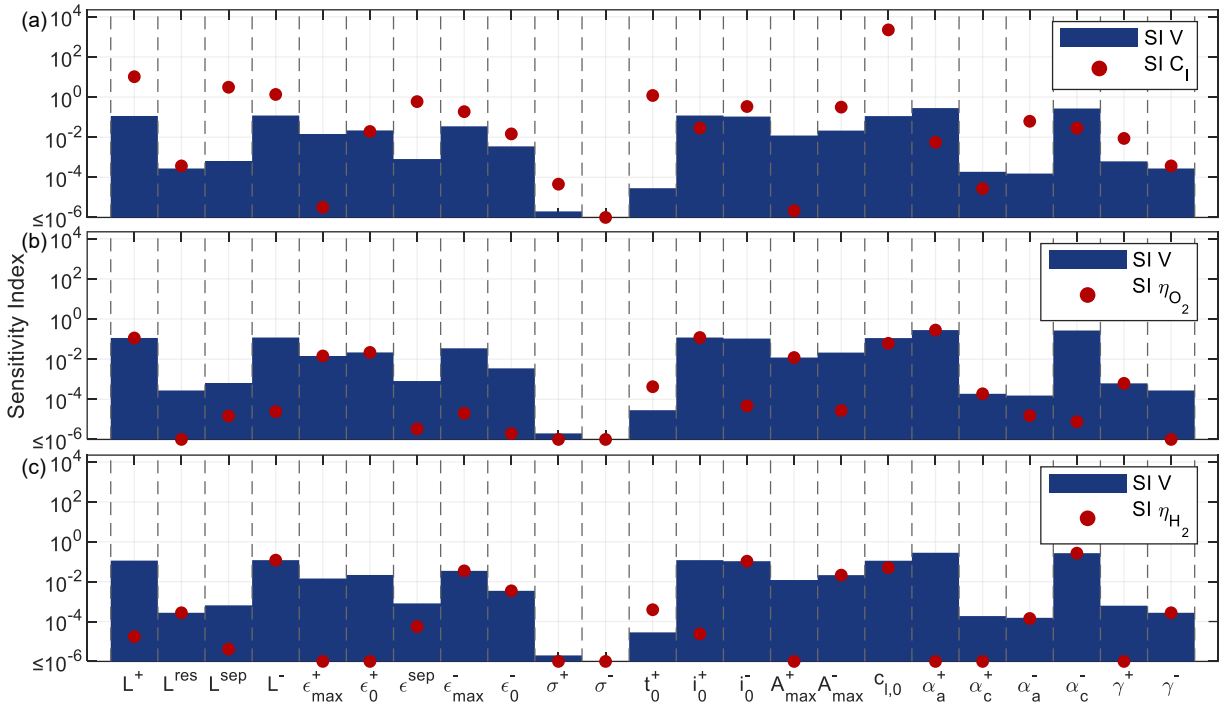

Fig. 6. Effect of parameter uncertainty on the model outputs. (a) Comparative analysis of the model sensitivity for V and c_l.(b) Comparative analysis of the model sensitivity for V and η_{O_2}.(c) Comparative analysis of the model sensitivity for V and η_{H_2}.

It has been demonstrated that only parameters related to concentration have a significant effect on electrolyte concentration and other types of parameters exert a negligible influence. The overpotential of side reactions is found to be significantly influenced solely by the parameters within the electrode region in which they occur. For instance, the parameters within the negative electrode region have been demonstrated to influence on the hydrogen evolution overpotential, while those within the positive electrode region have been shown to influence on the oxygen evolution overpotential. In the process of designing a parameter identification framework, the parameters that exhibit low sensitivity, such as σ^-, can be prioritized for exclusion. This reduction in identification dimension has been shown to improve efficiency [24]. In instances where the model proves incapable of accurately predicting specific side reactions, the parameters associated with these regions should be accorded a high priority for adjustment.

As demonstrated in Figure 6, the impact of parameter uncertainty on model output, e.g., c_l, η_{O_2}, and η_{H_2}, is illustrated. The y-axis employs a logarithmic scale to facilitate enhanced visualization of sensitivity indices across multiple orders of magnitude. It is important to note that the parameters with sensitivity indices below 10^{-6} are not displayed, as their effects are negligible. In conditions of sub-optimal charging, the sensitivity of each parameter to terminal voltage aligns with the conclusions in Section 5.1, with electrochemical parameters and capacity-related parameters exhibiting high sensitivity. Figure 6 comprises three subfigures, each of which illustrates the combination of terminal voltage and another target state. The findings indicate that for the electrolyte concentration state, the sensitivity index is approximately 1,000 times higher than that of the terminal voltage, primarily due to the concentration unit itself (mol/m³) being three orders of magnitude higher than the voltage (V). The units for oxygen evolution and hydrogen evolution overpotentials are consistent with voltage, and the parameter identifiability is higher than the impact of parameter uncertainty on the target state. This finding suggests that the parameter values obtained through terminal voltage identification are sufficient to accurately predict the internal state of the battery.

6. CONCLUSION

The paper conducts a sensitivity analysis on 23 parameters of the electrochemical model for lead-acid batteries. This analysis covers the sensitivity of terminal voltage under different discharge C-rates, as well as the sensitivity assessment of three target states, e.g., liquid electrolyte concentration, oxygen evolution overpotential, and hydrogen evolution overpotential, under constant current charging conditions. The primary conclusions of this study are as follows:

(1) It has been established that the sensitivity index of the parameters to terminal voltage is not generally lower than their sensitivity to other target states. This finding suggests that if a parameter can be effectively identified through changes in terminal voltage, it typically exerts a substantial influence on the overall behavior of the model. Conversely, if its sensitivity to terminal voltage is extremely low, its impact on the model output is often negligible.

(2) Among the 23 parameters, L^+, L^{res}, L^{sep}, L^-, ε^{sep}, i_o^+, i_o^-, α_a^+, α_c^+, α_a^-, α_c^-, γ^+, γ^-, c_0 are identified as a high-sensitivity parameter, while ε^+_{max}, ε^+_0, ε^-_{max}, ε^-_0, σ^+, σ^-, t^+_0, A^+_{max}, A^-_{max} consistently exhibited low-sensitivity. Consequently, when designing

a parameter identification framework, a stepwise identification strategy can be adopted. This strategy involves prioritizing the identification of high-sensitivity parameters, followed by the processing of low-sensitivity parameters once the high-sensitivity parameters have been determined. This method has the capacity to significantly reduce the dimension of the identification problem, improving identification efficiency and convergence.

(3) The sensitivity of parameters is critically dependent on specific operating conditions. Consequently, distinct operating conditions are required to identify different parameter types: capacity parameters necessitate low C-rate current conditions, whereas electrochemical parameters require high C-rate current conditions.

(4) The parameters exhibit non-uniform sensitivity distributions during discharge. The final stage of the discharge process is characterized by elevated sensitivity to parameters. The utilization of data from this region for parameter identification has been shown to result in a substantial reduction in the amount of data required, while maintaining accuracy. This approach effectively circumvents the risk of overfitting, which is often caused by the use of redundant data.

A parametric sensitivity analysis of a lead-acid battery electrochemical model was conducted in this work. In future studies, this analysis will be extended to multi-physics coupling conditions, such as an investigation based on an electrochemical-thermal coupled model. Furthermore, a parameter identification framework will be developed to achieve rapid and accurate parameter estimation.

DECLARATIONS

Author Contributions: H.R. writing—original draft preparation and data curation, K.D. investigation and writing—review and editing, J.L. Writing – review & editing, Validation, L.C. Validation, Software, H.Z Writing – review & editing, Investigation, Z.Z Supervision, Funding acquisition, Conceptualization.

Data Availability: Data will be made available on request.

Funding: This research was funded by Henan Province Science and Technology Research Projects (NO.242102241030).

REFERENCES

[1] Lopes P.P. and Stamenkovic V.R., 2020. Past, present, and future of lead-acid batteries. *Science* 369: 923-924.

[2] Dodo U.A., Salami B.A., Bashir F.M., Hamdoun H.Y., Rashed Alsadun I.S., Dodo Y.A., et al., 2024. Investigating the influence of erratic grid on stationary battery energy storage technologies in hybrid power systems: Techno-environ-economic perspectives. *Energy* 304: 132140.

[3] Asamoah G.A., Korsah M., Jeyasundar P.G.S.A., Ahmed M., Lau S.Y. and Danquah M.K., 2024. Nanotechnology-based lithium-ion battery energy storage systems. *Sustainability* 16: 9231.

[4] Thong P.T., Sim U., Kim Y.A., Jung S. and Jung H.-Y., 2025. Comparative insight into negative electrode performance in lead-acid and lead-carbon batteries under high-load and partial state-of-charge cycling profiles. *Journal of Energy Storage* 124: 116745.

[5] Tian A., He L., Ding T., Dong K., Wang Y. and Jiang J., 2025. A generic physics-informed neural network framework for lithium-ion batteries state of health estimation. *Energy* 332: 137215.

[6] Lyu C., Lai Q., Ge T., Yu H., Wang L. and Ma N., 2017. A lead-acid battery's remaining useful life prediction by using electrochemical model in the particle filtering framework. *Energy* 120: 975-984.

[7] Tian A., Ding T., He L., Dong K., Zhu L., Chang C., Lv L. and Jiang J., 2025. A novel method for joint estimation of SOC and SOP based on electrochemical modeling. *Journal of Energy Storage* 128: 117234.

[8] Lin W.-J. and Chen K.-C., 2022. Evolution of parameters in the Doyle-Fuller-Newman model of cycling lithium ion batteries by multi-objective optimization. *Applied Energy* 314: 118925.

[9] Zhou Y., Wang B.-C., Li H.-X., Yang H.-D. and Liu Z., 2021. A surrogate-assisted teaching-learning-based optimization for parameter identification of the battery model. *IEEE Transactions on Industrial Informatics* 17: 5909-5918.

[10] Tian A., Dong K., Yang X.-G., Wang Y., He L., Gao Y., et al., 2025. Physics-based parameter identification of an electrochemical model for lithium-ion batteries with two-population optimization method. *Applied Energy* 378: 124748.

[11] Li W., Cao D., Jöst D., Ringbeck F., Kuipers M., Frie F., et al., 2020. Parameter sensitivity analysis of electrochemical model-based battery management systems for lithium-ion batteries. *Applied Energy* 269: 115104.

[12] Dehghandorost H., Esfahanian V. and Chaychizadeh F., 2018. Uncertainty quantification and global sensitivity analysis of batteries: Application to a lead-acid battery. *Journal of the Electrochemical Society* 165: A3971-A3984.

[13] Chen J., Mattus S.P., Cao W., Sauer D.U. and Li W., 2025. Global sensitivity analysis towards non-invasive parameterization of the electrochemical-thermal model for lithium-ion batteries. *Advances in Applied Energy* 18: 100221.

[14] Iwakiri I.G.I., Delgado N.M. and Nogueira I.B.R., 2024. Introducing a new model for solid-state batteries: Parameter estimation and sensitivity analysis on diffusion, concentration, and electrochemical kinetics. *Electrochimica Acta* 508: 145202.

[15] Gu W.B., Wang C.Y. and Liaw B.Y., 1997. Numerical modeling of coupled electrochemical and transport processes in lead-acid batteries. *Journal of the Electrochemical Society* 144: 2053-2061.

[16] Esfahanian V., Shahbazi A.A. and Torabi F., 2019.

A real-time battery engine simulation tool (BEST) based on lumped model and reduced-order modes: Application to lead-acid battery. *Journal of Energy Storage* 24: 100780.

[17] Shi M., Yuan J., Dong L., Zhang D., Li A. and Zhang J., 2020. Combining physicochemical model with the equivalent circuit model for performance prediction and optimization of lead-acid batteries. *Electrochimica Acta* 353: 136567

[18] Ansari A.B., Esfahanian V. and Torabi F., 2016. Discharge, rest and charge simulation of lead-acid batteries using an efficient reduced order model based on proper orthogonal decomposition. *Applied Energy* 173: 152-167.

[19] Esfahanian V., Ansari A.B. and Torabi F., 2015. Simulation of lead-acid battery using model order reduction. *Journal of Power Sources* 279: 294-305.

[20] Sulzer V., Chapman S.J., Please C.P., Howey D.A. and Monroe C.W., 2019. Faster lead-acid battery simulations from porous-electrode theory: Part I. Physical model. *Journal of the Electrochemical Society* 166: A2363-A2371.

[21] Sulzer V., Chapman S.J., Please C.P., Howey D.A. and Monroe C.W., 2019. Faster lead-acid battery simulations from porous-electrode theory: Part II. Asymptotic analysis. *Journal of the Electrochemical Society* 166: A2372-A2382.

[22] Li W., Demir I., Cao D., Jöst D., Ringbeck F., Junker M., et al., 2022. Data-driven systematic parameter identification of an electrochemical model for lithium-ion batteries with artificial intelligence. *Energy Storage Materials* 44: 557-570.

[23] Wang Y., Lin N., Liu D., Liu Z., Li J. and Lin H., 2024. Tin dioxide coated rice husk silica as lead-acid battery positive additive for enhancing the performance under power-intensive applications. *Journal of Power Sources* 602: 234345.

[24] Xu L., Lin X., Xie Y. and Hu X., 2022. Enabling high-fidelity electrochemical P2D modeling of lithium-ion batteries via fast and non-destructive parameter identification. *Energy Storage Materials* 45: 952-968.